

Shear Viscosity of Clay-like Colloids: Computer Simulations and Experimental Verification

Martin Hecht,¹ Jens Harting,¹ Markus Bier,² Jörg Reinshagen,³ and Hans J. Herrmann^{1,4}

¹ Institute for Computational Physics, Pfaffenwaldring 27, 70569 Stuttgart, Germany

² Max-Planck-Institut für Metallforschung,

Herrnbergstraße 3, 70569 Stuttgart, Germany

and Institut für Theoretische und Angewandte Physik,

Universität Stuttgart, Pfaffenwaldring 57, 70569 Stuttgart, Germany

³ Institute of Ceramics in Mechanical Engineering,

University of Karlsruhe (TH), Karlsruhe, 76131 Germany

⁴ Departamento de Física, Universidade Federal do Ceará Campus do Pici, 60451-970 Fortaleza CE, Brazil
(Dated: December 20, 2018)

Abstract.

Dense suspensions of small strongly interacting particles are complex systems, which are rarely understood on the microscopic level. We investigate properties of dense suspensions and sediments of small spherical Al_2O_3 particles in a shear cell by means of a combined Molecular Dynamics (MD) and Stochastic Rotation Dynamics (SRD) simulation. We study structuring effects and the dependence of the suspension's viscosity on the shear rate and shear thinning for systems of varying salt concentration and pH value. To show the agreement of our results to experimental data, a relation between bulk pH value and surface charge of spherical colloidal particles is obtained within Debeye-Hückel theory in conjunction with a 2pK charge regulation model.

PACS numbers: 47.57.J-, 47.11.-j, 47.57.Qk, 77.84.Nh

I. INTRODUCTION

We simulate clay-like colloids, for which in many cases the attractive Van-der-Waals forces are relevant. They are sometimes called "peloids" (Greek: clay-like). In soil mechanics there is a need to better understand materials containing particles of m size and below. As a model system we have chosen a suspension of Al_2O_3 particles with a diameter of 0.37 nm. Al_2O_3 is not only a cheap testing material for investigations related to soil mechanics, but it is also an important material for ceramics. In process engineering one of the basic questions is, how to obtain components of a predefined shape. Wet processing of suspensions, followed by a sinter process is a common practice here. Nevertheless, to optimize the production process and to improve the homogeneity and strength of the fabricated workpiece one has to understand the complex rheological behavior of the suspension and its relation to the microscopic structure. This knowledge in turn can be applied to soil mechanics. Shear thinning as observed in our simulations and experiments is a very important mechanism for the dynamics of landslides making them more dangerous.

In this paper we present our simulation results of sheared suspensions of Al_2O_3 particles. The overall behavior is strongly determined by the effective interaction potential between the particles in the suspension. The potentials can

be related to experimental conditions within Debeye-Hückel theory, and thus we can compare our simulation results to experimental data.

Our paper is organized as follows: first we shortly describe our molecular dynamics (MD) implementation followed by a short sketch of the stochastic rotation dynamics (SRD) simulation method, and a description of how we have implemented our shear cell. The simulation method is described in detail in ref. [1]. Then we describe the so called 2pK charge regulation model which relates our simulation parameters with the pH-value and ionic strength I adjusted in the experiment. A short description of the simulation setup and of the experiments carried out follows. After that we present our simulation results and compare them to the experimental data. Finally a summary is given.

II. MOLECULAR DYNAMICS

We study colloidal particles, composing the solid fraction, suspended in a liquid solvent. The colloidal particles are simulated with molecular dynamics (MD), whereas the solvent is modeled with stochastic rotation dynamics (SRD) as described in Sec. III.

In the MD part of our simulation we include effective electrostatic interactions and van der Waals attraction, a lubrication force and Hertzian contact forces. The electrostatic and van der Waals potential are usually referred to

as D LVO potentials [2, 3, 4], which capture quite well the static properties of colloidal particles in aqueous suspensions. The first component is the screened Coulomb term

$$V_{\text{Coul}} = \frac{h}{r} \left(\frac{2+}{1+} \frac{d}{r} \frac{4k_B T}{ze} \tanh \frac{ze}{4k_B T} \right) \exp \left(-\frac{d}{r} \right); \quad (1)$$

where d denotes the particle diameter and r is the distance between the particle centers. e is the elementary charge, T the temperature, k_B the Boltzmann constant, and z is the valency of the ions of added salt. Within D LVO theory one assumes linear screening, mainly by one species of ions with valency z (e.g. $z = +1$ for NH_4^+). The first fraction in Eq. 1 is a correction to the original D LVO potential, which takes the surface curvature into account and is valid for spherical particles [5].

The effective surface potential is the electrostatic potential at the border between the diffuse layer and the compact layer, it may therefore be identified with the ϕ -potential. It includes the effect of the bare charge of the colloidal particle itself, as well as the charge of the ions in the Stern layer, where the ions are bound permanently to the colloidal particle. In other words, D LVO theory uses a renormalized surface charge, which we determine by the model described in Sec. IV.

λ_D is the inverse Debye length defined by $\lambda_D^2 = 8 \cdot \kappa_B T / (4 \cdot \epsilon_0 \cdot \epsilon_r)$, with the ionic strength I . The Debye length $\lambda_D = \frac{e^2}{4 \cdot \epsilon_0 \cdot \epsilon_r}$ measures the distance at which the electrostatic interaction of two elementary charges amounts $1 = k_B T / \epsilon_0$. ϵ_0 is the permittivity of the vacuum, ϵ_r the relative dielectric constant of the solvent (we use 81 for water, i.e., $\lambda_D = 7 \text{ \AA}$ for room temperature).

The Coulomb term of the D LVO potential competes with the attractive van der Waals term

$$V_{\text{vdW}} = \frac{h}{12} \left(\frac{d^2}{r^2} + \frac{d^2}{r^2} \right) + 2 \ln \left(\frac{r^2 - d^2}{r^2} \right); \quad (2)$$

$A_H = 4.76 \cdot 10^{20} \text{ J}$ is the Hamaker constant [6] which involves the polarizability of the particles. It is kept constant in our simulations since it only depends on the material of the particles and on the solvent.

Long range hydrodynamic interactions are taken into account in the simulation for the uid as described below. This can only reproduce interactions correctly down to a certain length scale. On shorter distances, a lubrication force has to be introduced explicitly in

the molecular dynamics simulation. The most dominant mode, the so-called squeezing mode, is an additional force

$$F_{\text{lub}} = (\nu_{\text{rel}}; \dot{\tau}) \frac{6}{r} \frac{r_{\text{red}}^2}{r_1 r_2}; \quad (3)$$

$$\text{with } r_{\text{red}} = \frac{r_1 r_2}{r_1 + r_2} \quad (4)$$

between two spheres with radii r_1 , r_2 and the relative velocity ν_{rel} . $\dot{\tau}$ is the dynamic viscosity of the uid. In contrast to the D LVO potentials the lubrication force is a dissipative force. When two particles approach each other very closely, this force becomes very large. To ensure numerical stability of the simulation, one has to limit F_{lub} . We do this by introducing a small cut-off radius r_{sc} . Instead of calculating $F_{\text{lub}}(r)$ we take the value for $F_{\text{lub}}(r + r_{\text{sc}})$. In addition, since the force decays for large particle distances, we can introduce a large cut-off radius r_{lc} for which we assume $F_{\text{lub}}(r) = 0$ if $r > r_{\text{lc}}$. As the intention of F_{lub} is to correct the finite resolution of the uid simulation, r_{sc} and r_{lc} have to be adjusted in a way that the dynamic properties, i.e., the viscosity of a simulated particle suspension with weak D LVO interactions fits the measurements. It turns out that $r_{\text{sc}} = 1.05(r_1 + r_2)$ and $r_{\text{lc}} = 2.5(r_1 + r_2)$ work best.

Finally we use a Hertz force described by the potential

$$V_{\text{Hertz}} = K (d - r)^{5/2} \quad \text{if } r < d; \quad (5)$$

where K is the constant which describes the elasticity of the particles in the simulation. The Hertz force avoids that the particles penetrate each other. It also contains a damping term in normal direction,

$$F_{\text{Damp}} = (\nu_{\text{rel}}; \dot{\tau}) \frac{p}{r} \frac{r}{r_1 r_2}; \quad (6)$$

with a damping constant p .

Since in this work no stress perpendicular to the shear direction is applied, the tangential forces at the particle surface are not of essential importance. To verify this, we have increased the spacial resolution of the uid simulation, included tangential forces on the particles and allowed particle rotations. Even though the computational effort was considerably higher and one could expect that more effects on the length scale below the particle diameter could be covered. However one could observe only a change of some percent in the viscosity and in the velocity profile. Due to the D LVO potential and the lubrication force the particles very rarely get into contact as long as no confining stress is applied. The only case, in which particles really

touch each other, would be if the potential is close to zero at a certain pH value. This pH value is called "isoelectric point". It depends on the material of the suspended particles and on the solvent. For our system it is at pH = 8.7 [4]. In experiments close to the isoelectric point a solid fraction immediately coagulates out and sediments. In the simulation one ends up with only one big cluster in the simulation volume, which corresponds to a part of a seen in the experiment.

For this study we do not apply tangential forces and thus, having only central forces, we could neglect rotation of the particles. This reduces the computational cost.

III. STOCHASTIC ROTATION DYNAMICS (SRD): SIMULATION OF THE FLUID

The stochastic rotation dynamics method (SRD) was first introduced by Malevanets and Kapral [7, 8]. It is a promising tool for a coarse-grained description of a fluctuating solvent. The method is also known as "real-coded lattice gas" [9] or as "multiparticle-collision dynamics" (MPCD) [10, 11]. It is based on so-called uid particles with continuous positions and velocities. Each time step is composed of two simple steps: One streaming step and one interaction step. In the streaming step the positions of the uid particles are updated as in the Euler integration scheme known from Molecular Dynamics simulations:

$$r_i(t + \Delta t) = r_i(t) + v_i(t); \quad (7)$$

where $r_i(t)$ denotes the position of the particle i at time t , $v_i(t)$ its velocity at time t and Δt is the time step used for the SRD simulation. After updating the positions of all uid particles they interact collectively in an interaction step which is constructed to preserve momentum, energy and particle number. The uid particles are sorted into cubic cells of a regular lattice and only the particles within the same cell are involved in the interaction step. First, their mean velocity $u_j(t^0) = \frac{1}{N_j(t^0)} \sum_{i=1}^{N_j(t^0)} v_i(t)$ is calculated, where $u_j(t^0)$ denotes the mean velocity of cell j containing $N_j(t^0)$ uid particles at time $t^0 = t + \Delta t$. Then, the velocities of each uid particle in cell j are updated as:

$$v_i(t + \Delta t) = u_j(t^0) + \gamma_j(t^0) [\mathbf{f}_i(t) - u_j(t^0)]; \quad (8)$$

$\gamma_j(t^0)$ is a rotation matrix, which is independently chosen randomly for each time step and

each cell. We use rotations about one of the coordinate axes by an angle θ , with θ random. The coordinate axis as well as the sign of the rotation are chosen by random, resulting in 6 possible rotation matrices. The mean velocity $u_j(t)$ in the cell j can be seen as streaming velocity of the uid at the position of the cell j at the time t , whereas the difference $[\mathbf{f}_i(t) - u_j(t^0)]$ entering the interaction step can be interpreted as a contribution to the thermal fluctuations [19].

The method just described is able to reproduce hydrodynamics and thermal fluctuations. To couple the colloidal particles to the streaming field of the solvent, we modify the original SRD algorithm as described in the following: the colloidal particles are sorted into the SRD cells as well and their velocity enters into the calculation of the mean velocity $u_j(t)$ in cell j . Since the mass of the uid particles is much smaller [20] than the mass of the colloidal particles, we have to use the mass of each particle | colloidal or uid particle| as a weight factor when calculating the mean velocity

$$u_j(t^0) = \frac{1}{M_j(t^0)} \sum_{i=1}^{N_X(t^0)} m_i v_i(t) m_i; \quad (9)$$

$$\text{with } M_j(t^0) = \sum_{i=1}^{N_X(t^0)} m_i; \quad (10)$$

where we sum over all colloidal and uid particles in the cell, so that $N_j(t^0)$ is the total number of both particles together. m_i is the mass of the particle with index i and therefore $M_j(t^0)$ gives the total mass contained in cell j at the time $t^0 = t + \Delta t$. The update rule for the particle velocities $v_i(t)$ and positions $r_i(t + \Delta t)$, which we apply, is summarized in Eqs. 7{10}. This method to couple some embedded material to the SRD simulation is described for different applications in the literature [12, 13].

In ref. [1] we have described a simple method to introduce shear at the uid boundary by adding a velocity offset to all uid particles reflected at the shear plane. From a constant velocity offset v one can calculate the mean shear force

$$F_S = \frac{1}{m_i} \sum_{i=1}^{N_X(t^0)} \frac{v_i(t)}{L} + \dots; \quad (11)$$

where L denotes the average number of uid particles crossing through the shear plane in one time step and $\langle \dots \rangle$ stands for a time average. L can be expressed by the mean free path and the number density of uid particles. This would be a force driven shear, where one has only indirect control on the shear rate _ or

the shear velocity v_s respectively. Therefore, we modify the mean velocity $u_j(t^0)$ in the cells close to the shear plane by changing the velocity of each uid particle as well as the velocity of the colloidal particles contained in that specific cell by the difference $v_s - u_j(t^0)$. By construction the mean velocity in these cells is equal to the shear velocity v_s after that step. At the wall itself we implement no-slip boundary conditions for the uid and for the colloidal particles. The boundary in the direction of the shear profile (direction of the velocity gradient) is chosen to be non-periodic. By doing so, we can also observe phenomena like wall-slip, non-linear velocity profiles or density profiles in our shear cell. In the case of a non-linear velocity profile the viscosity is not well defined. We extract the central region of the profile where it is in first approximation linear and estimate there an averaged viscosity. This is the ratio of the velocity gradient and the shear force which can be calculated in analogy to Eq. (11) by carrying out the sum over all velocity changes made. The region where we estimate the velocity gradient is half the system size.

IV. THE CHARGE REGULATION MODEL

To determine the effective surface potential which enters the DLVO potential, we use the model described in the following. In reality, the surface charge is achieved by adsorption and desorption of charge determining ions leading to an electrostatic potential difference between surface and bulk which in turn influences ion adsorption. A full description of this regulation of surface charges requires two parts: the first part describes the relation between surface charge density and surface potential due to the electrolytic environment, whereas the second part quantifies the ion adsorption depending on the surface concentration of charge determining ions.

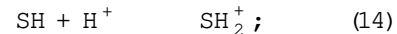
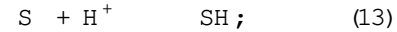
Concerning the first part, a relation between the surface charge density and the surface potential of a charged spherical colloidal particle of radius R immersed in an electrolytic environment of relative dielectric constant ϵ_r and ionic strength I is given within Debye-Hückel theory [14, 15] by

$$= \frac{R}{\epsilon_0 \epsilon_r (1 + R)} : \quad (12)$$

As mentioned above, we consider the Stern layer as a part of the surface charge and thus,

we can identify the effective surface potential in DLVO theory with the ϕ -potential.

In the second part of our model, the adsorption of charge determining ions on the surface of the colloidal particle is described by assuming that the only mechanism of adsorption is that of protons (H^+) on surface sites (S). It turned out that this assumption leads to reasonable results for surfaces made of Al_2O_3 . Adsorption is described by the two chemical reactions [16]



with the two reaction constants

$$K_1 = \frac{[S][H^+] \exp(-e)}{[SH]}; \quad (15)$$

$$K_2 = \frac{[SH][H^+] \exp(-e)}{[SH_2^+]}: \quad (16)$$

In terms of the surface site concentrations, the total number of surface sites per area and the surface charge density are given by $N_s = [S] + [SH] + [SH_2^+]$ and $= e[S] + e[SH_2^+]$, respectively. Defining $pK_1 = \log_{10}(K_1)$ and $pK_2 = \log_{10}(K_2)$ yields the point of zero charge pH_z , i.e., the pH value of vanishing surface charge, as $pH_z = \frac{1}{2}(pK_1 + pK_2)$. The surface site density N_s and the difference $pK = pK_1 - pK_2$ are treated as adjustable parameters.

The above equations lead to the relation

$$\epsilon N_s = \frac{\sinh(\frac{N}{N_s}e)}{1 + \cosh(\frac{N}{N_s}e)} \quad (17)$$

with the Nernst potential $N = \ln(10)(pH_z - pH)$ and $= 2 \cdot 10^{-\frac{pK}{2}}$.

Equations (12) and (17) can be solved self-consistently for ϕ as a function of pH. For our system of Al_2O_3 particles we find $pK = 4.2$ and $N_s = 0.22 \text{ nm}^{-2}$. With these values the measured potential of 52 mV at pH = 6, $I = 0.01 \text{ mol/l}$ and up to 120 mV at pH = 4, $I = 0.01 \text{ mol/l}$ can be reproduced best.

V. SIMULATION SETUP

The colloidal particles in our simulation are represented by three dimensional spheres. We simulate 9241 spheres, each of diameter 0.37 m. The volume we usually simulate is 17.76 m long in x-direction, 8.88 m in z-direction, and 4.44 m in y-direction. This results in an average volume fraction of $= 35\%$. Our shear direction is the x-direction and the

velocity gradient of the shear flow points in z -direction; in other words we shear the upper and lower xy -plane with respect to each other in x -direction. We use periodic boundaries in x - and y -direction and closed boundaries in z -direction.

V I. EXPERIMENTAL SET UP

Experiments are carried out with high purity (99,97%) Al_2O_3 powder (RCHP DBM, Baikowski Malako Industries, Inc., USA). The powder is suspended in bidistilled water (Merck, Germany). The suspension is then dispersed with alumina balls in a ceramic container for 24 h at a small rotational speed to keep the abrasion low. Subsequently, the suspension is degassed at 50 mbar under agitation. Then, in order to reduce the ionic strength to the desired degree, the suspension is purified by the dialysis technique. In this way the majority of ions are removed and a background electrolyte of a very low salt concentration ($5 \times 10^4 \text{ mol/l}$) is obtained for suspensions of high solids loading. Starting from this master suspension, suspensions with increased ionic strength are obtained by adding different amounts of dry ammonium chloride NH_4Cl (Merck, Germany). The pH of the suspensions is adjusted to $\text{pH} = 6$ with 0.1 and 1 mol/l hydrochloric acid HCl (Merck, Germany), if necessary. Thereby the ionic strength and pH are revised by use of a laboratory pH- and conductivity meter (InoLab pH/Cord Level 2, WTW GmbH, Germany). The electrophoretic mobility of dilute suspensions is measured with a Coulter Elsa 440 SX. The ion concentrations of selected ions are measured before and after dialysis using Inductively Coupled Plasma Optical Emission Spectroscopy (ICP-OES, Model JY 70 plus, France). The suspensions are characterized using a shear rate controlled rheometer (Viscolab LC 10, Physica, Germany) with a cup and bob or a double gap geometry. Shear rate controlled experiments are performed at a constant temperature of 20 °C. The suspensions are sheared at a constant shear rate of $\dot{\gamma} = 300 \text{ s}^{-1}$ before starting the actual ramp measurement. In the experiments the shear rate is increased up to $\dot{\gamma} = 4000 \text{ s}^{-1}$ and decreased again to zero. When the suspensions are pre-sheared an occurring discrepancy between the measured viscosity in the increasing ramp and the decreasing one can be minimized. A detailed description of the experiments will be published elsewhere [17].

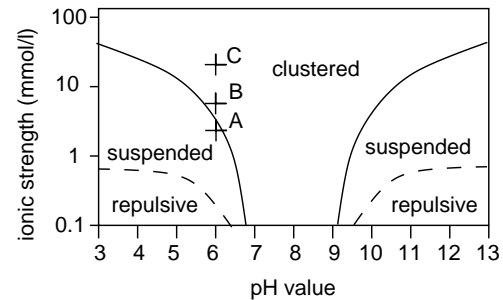


FIG. 1: Schematic phase diagram for volume fraction $\phi = 35\%$ in terms of pH-value and ionic strength involving three different phases: A clustering regime due to van der Waals attraction, stable suspensions where the charge of the colloidal particles prevents clustering, and a repulsive structure for further increased electrostatic repulsion. This work concentrates on state A ($\text{pH} = 6$, $I = 3 \text{ mmol/l}$) in the suspended phase, state B ($\text{pH} = 6$, $I = 7 \text{ mmol/l}$) close to the phase border but already in the clustered phase, and state C ($\text{pH} = 6$, $I = 25 \text{ mmol/l}$) in the clustered phase.

V II. RESULTS

A. Phase diagram

Depending on the experimental conditions, one can obtain three different phases: A clustered region, a suspended phase, and a repulsive structure. The charge regulation model allows us to quantitatively relate the interaction potentials to certain experimental conditions. A schematic picture of the phase diagram is shown in Fig. 1. Close to the isoelectric point ($\text{pH} = 8.7$), the particles form clusters for all ionic strengths since they are not charged. At lower or higher pH values one can prepare a stable suspension for low ionic strengths because of the charge, which is carried by the colloidal particles. At even more extreme pH values, one can obtain a repulsive structure due to very strong electrostatic potentials (up to $= 170 \text{ mV}$ for $\text{pH} = 4$ and $I = 1 \text{ mmol/l}$, according to our model). The repulsive structure is characterized by an increased shear viscosity. In the following we focus on three states: State A ($\text{pH} = 6$, $I = 3 \text{ mmol/l}$) is in the suspended phase, state B ($\text{pH} = 6$, $I = 7 \text{ mmol/l}$) is a point already in the clustered phase but still close to the phase border, and state C ($\text{pH} = 6$, $I = 25 \text{ mmol/l}$) is located well in the clustered phase.

Some typical examples for the different phases are shown in Fig. 2a)-(d). These exam-

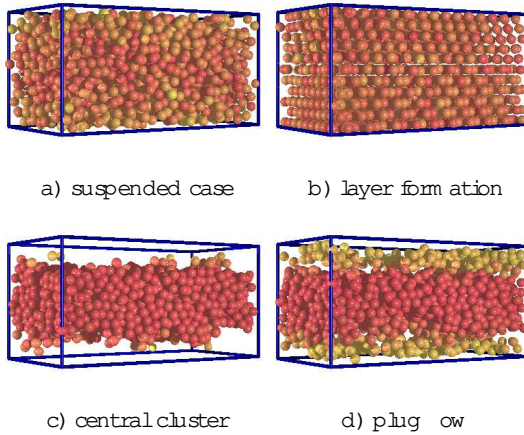


FIG. 2: Images of four different cases. For better visibility we have chosen smaller systems than we usually use for the calculation of the viscosity. The colors denote velocities: Dark particles are slow, bright ones move fast. The potentials do not correspond exactly to the cases A (C) in Fig.1, but they show qualitatively the differences between the different states:

- a) Suspension like in state A, at low shear rates.
- b) Layer formation, which occurs in the repulsive regime, but also in the suspension (state A) at high shear rates.
- c) Strong clustering, like in state C, so that the single cluster in the simulation is deformed.
- d) Weak clustering close to the phase border like in state B, where the cluster can be broken into pieces, which follow the flow of the fluid (plug flow).

These are meant to be illustrative only and do not correspond exactly to the cases A (C) in Fig.1 denoted by uppercase letters. In the suspended case (a), the particles are mainly coupled by hydrodynamic interactions. One can find a linear velocity profile and a slight shear thinning. If one increases the shear rate $\dot{\gamma} > 500/s$, the particles arrange in layers. The same can be observed if the Debye-screening length of the electrostatic potential is increased (b), which means that the solvent contains less ions ($I < 0.3 \text{ mMol/l}$) to screen the particle charges. On the other hand, if one increases the salt concentration, electrostatic repulsion is screened even more and attractive van der Waals interaction becomes dominant ($I > 4 \text{ mMol/l}$). Then the particles form clusters (c), and viscosity rises. A special case, called 'plug flow', can be observed for high shear rates, where it is possible to tear the clusters apart and smaller parts of them follow with the flow of the solvent (d). This happens in our simulations for $I = 25 \text{ mMol/l}$ (state C) at a shear rate of $\dot{\gamma} > 500/s$. However, as long as there are only one or two big clusters in the system, it is too

small to expect quantitative agreement with experiments. In these cases we have to focus on state B ($I = 7 \text{ mMol/l}$) close to the phase border.

In our simulations we restrict ourselves to the region around $\text{pH} = 6$ where we find the phase border between the suspended region and the clustered regime at about $I = 4 \text{ mMol/l}$ in the simulations as well as in the experiments. Also the shear rate dependence of the viscosity is comparable in simulations and experiments as discussed in Sec. V IIC.

B. Total Energy

In our simulations we calculate the total energy, because it can be used as a tool to check if the response of the simulation to the variation of any parameter is consistent with the expectations, e.g., a decrease of the surface charge on the colloidal particles should cause the minimum of the Debye potential to become deeper and thus decrease the total energy (but if the total energy increases, this can be an indication for numerical instabilities).

The total energy comprises the kinetic energy of both fluid and colloidal particles, including thermal motion on the microscopic level, as well as the potential energy due to Coulomb repulsion, van der Waals attraction, and Hertz contact forces. Our simulations are carried out at room temperature ($T = 295 \text{ K}$) and constant volume fraction. Supposing a linear velocity profile, the kinetic energy increases quadratically with the shear rate $\dot{\gamma}$. This can be observed if the electrostatic repulsion is, on the one hand, strong enough to prevent cluster formation due to van der Waals attraction and, on the other hand, weak enough, so that the colloidal particles can move relatively freely without undergoing a glass transition or crystallization.

If the interactions are strongly repulsive, i.e., in the case of very low salt concentration, where the Debye-screening length is large, one can see an extra contribution of the electrostatic repulsion to the total energy. If the volume fraction is low, the particles can still find a configuration, in which the mean nearest neighbor distance is larger than the interaction range of the repulsion. But, if the volume fraction is increased, the particles have to be packed closer, which leads to a constant offset to the total energy. It only depends on the potentials and on the volume fraction, but not on the shear rate.

By introducing shear the particles are forced to arrange in layers parallel to the shear plane.

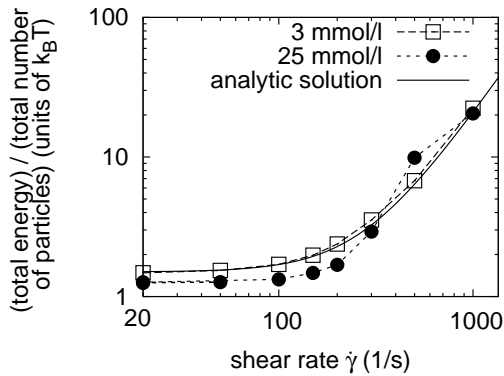


FIG. 3: Total energy depending on the shear rate γ for the states A ($I = 3 \text{ mmol/l}$) and C ($I = 25 \text{ mmol/l}$) of Fig.1. In state A the system is a stable suspension, in state C cluster formation reduces the total energy at low shear rates. At $\gamma = 500 \text{ s}^{-1}$, the cluster can be broken up into two parts moving in opposite directions. The two solid bodies have a larger kinetic energy than the suspension with a linear velocity profile. This explains the crossover of the two curves. For even higher γ , the clusters are broken up in more pieces leading ultimately to the same structure as for the suspended state A. The energy axis has been scaled by the total number of particles (uid particles plus colloidal particles) and plotted in units of $k_B T$. The solid line is the analytical solution (Eq.18) for a linear velocity profile, the dashed lines are a guide to the eye.

In hard sphere systems of large volume fractions shear can become impossible at a sharp phase border. The analogous effect in our particle suspension leads to an increase of viscosity for low salt concentrations (see Sec. V IIC). Strictly speaking there is no sharp phase transition in the classical sense from the suspended regime to the repulsive one (see Fig.1), but a rather continuous change in the behavior of the suspension.

In a similar way as for repulsive interactions, one can understand the negative energy contribution in the case of high salt concentrations: The DLVO potentials contain a minimum where attractive Van der Waals interaction is stronger than electrostatic repulsion. Then the particles form clusters and 'try' to minimize their energy. In Fig.3 for small shear rates the values for the energy in the clustered case of state C ($I = 25 \text{ mmol/l}$) is lower than for the suspended case of state A ($I = 3 \text{ mmol/l}$). We have plotted the total energy divided by the total number of all particles (uid particles plus colloidal particles) in units of $k_B T$. For $\gamma = 0$ the energy per particle approaches $\frac{3}{2}k_B T$ as one would expect in 3D. The solid line in Fig.3 is the sum of $\frac{3}{2}k_B T$ per particle with the kinetic

energy of a uid with a linear velocity profile:

$$E_{\text{tot}} = \frac{3}{2}k_B T N_{\text{tot}} + \frac{1}{24}V \gamma^2 L_z^2; \quad (18)$$

where N_{tot} is the total number of both, uid and colloidal particles, V denotes the volume of the simulated system, γ the averaged mass density of the suspension, and L_z is the extension in z-direction (perpendicular to the shear plane). State A coincides very well with this curve.

For state C the behavior is shear rate dependent: In contrast to the repulsive case, clusters can be broken up. This happens at a shear rate $\gamma = 500 \text{ s}^{-1}$ (see Fig.3) where one obtains two clusters moving in opposite directions. Since in this case the resistance of the system decreases, the velocity of the two clusters becomes larger. Since both clusters are moved as a whole, their energy even becomes larger than in the suspended case. If one further increases the shear rate, no (big) clusters can form anymore and the energies for both salt concentrations are nearly the same, and correspond to the kinetic energy of a suspension with a nearly linear velocity profile. For $\gamma = 1000 \text{ s}^{-1}$ state C coincides with the analytic curve.

C. Shear Profile and Shear Viscosity

In each of the three phases a typical velocity profile of the shear flow occurs. In the suspended phase one finds a linear velocity profile (Fig.4a) with nearly Newtonian flow. The particles are distributed homogeneously, thus the density profile is structureless (Fig.5a). The motion of the particles is only weakly coupled by the hydrodynamic forces. At high enough shear rates ($\gamma > 500$) the particles arrange in layers parallel to the shear plane, as can be seen in the density profile Fig.5b), too. This arrangement minimizes collisions between the particles. As a result, the shear viscosity decreases as shown in Fig.6, which we discuss more in detail below. Shear induced layer formation has been reported in literature for different systems. Vermant and Solon have reviewed this topic recently [18].

In the clustered phase, the clusters move in the uid as a whole. They are deformed, but since the inter-particle forces are stronger than the hydrodynamic forces, the cluster moves more like a solid body than like a uid. Often there is one big cluster that spans the whole system. The density profile (Fig.5c)) increases in the central region and decays at the regions close to the border, since particles from there

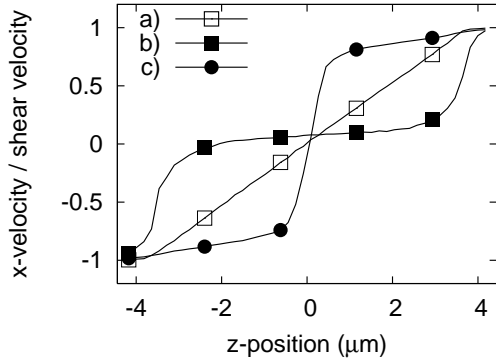


FIG. 4: Profiles of tangential velocity component (v_x) in normalized direction (z):

- a) Linear profile in the suspended regime, state A of Fig.1 ($I = 3 \text{ m m o l/l}$) at $\tau = 500\text{s}$.
- b) Cluster formation in state C ($I = 25 \text{ m m o l/l}$) at $\tau = 100\text{s}$. In principle one could determine the viscosity of one single cluster from the central plateau, but this is not the viscosity found in experiments. There, one measures the viscosity of a paste consisting of many of these clusters.
- c) Same as case b) but with higher shear rate ($500/\text{s}$). Hydrodynamic forces are large enough to break the cluster into two pieces.

The velocity axis is scaled with the shear velocity v_s for better comparability.

join the central cluster. When averaging the velocity profile in the shear flow, one finds a very small velocity gradient in the center of the shear cell and fast moving particles close to the wall, where the shear is imposed (Fig.4b)). The velocity profile is non-linear on the length scale of the simulations. In the experiment the physical dimensions are much larger and therefore the velocity profile can become approximately linear again if the system consists of many large clusters. However, due to the computational effort in simulations it is today impossible to measure the shear viscosity for these strongly inhomogeneous systems. We have scaled our system by a factor of 2 in x and z -direction (keeping the volume fraction $\phi = 35\%$ constant), but we still observe one big cluster after some hundreds of SRD time steps, i.e., finite size effects are still present in our simulations.

Closer to the phase border clusters can then be broken up into small pieces by the hydrodynamic forces at least for high shear rates. In state C of Fig.1 this happens for the first time at $\tau = 500\text{s}$, so that one can find two clusters in the system moving in opposite directions. The velocity profile of this case is shown in Fig.4c). For even higher shear rates or closer to the phase border (e.g. state B), the clusters are broken into smaller pieces. Then, they

move in the shear flow with an approximately linear velocity profile. Due to van der Waals attraction the system resists with stronger shear forces and the viscosity is higher than in the suspended case (Fig.6).

In Fig.6 the simulation results are shown together with the experimental results, both for the two cases of a slightly clustered system in state B ($I = 7 \text{ m m o l/l}$) and a suspension (state A, $I = 3 \text{ m m o l/l}$). For the suspension (state A) the viscosity decreases with the shear rate ("shear thinning"). The experimental data and the simulation are consistent within the accuracy of our model. There are several reasons for which our model does not fit exactly the measurements: The most insecure factor which enters into the comparison is the measurement of the τ -potential. Starting from this point we set up our charge regulation model to extrapolate to different salt concentrations, assuming two reactions being the only processes that determines the surface charge of the colloidal particles. Furthermore, we have monodisperse spheres, which is another simplification in our model. Then, the lubrication force as a correction for the finite resolution of the uid method can only recover to a certain degree the hydrodynamics on smaller length scales than the cell size of the uid simulation [21]. Finally, one has to keep in mind that the viscosity of the suspension can be varied by more than one order of magnitude, e.g., by changing the ionic strength. In this context the deviations between simulation and experiment are small.

For the slightly clustered case (state B) an increase of the shear viscosity, compared to the suspended case, can be observed in the experiment as well as in the simulations. Shear thinning becomes more pronounced, because clusters are broken up, as mentioned above. However, the shear rate dependence is stronger in the simulations than in the experiment. This can be the first indication of finite size effects. We have studied the dependence of the simulated shear viscosity in dependence of the system size. The effect is most important for low shear rates and thus we carried out several simulations for state A at $\tau = 20\text{s}$ and for state B at $\tau = 20\text{s}$ [22]. In Fig.7 we plotted the squared relative deviation between simulation and measurements against the system size. The deviation becomes smaller for larger system sizes, but to reach in state B the same accuracy as in state A one would have at least to double the system size in each dimension. It then takes approximately twice as long for the system to relax to a steady state, resulting in a factor of 16 in the computational effort. Each

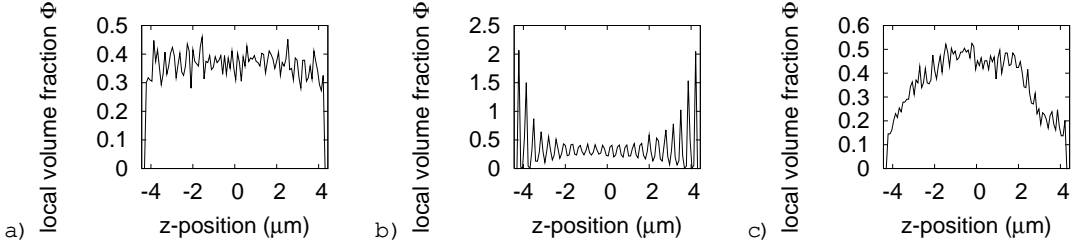


FIG. 5: Density profiles: a) Suspended case: State A in Fig. 1 ($I = 3 \text{ mmol/l}$), at low shear rates ($\dot{\gamma} = 50 \text{ s}^{-1}$). The density distribution is homogeneous.
 b) Shear induced layer formation: This is state A as in graph a) of this figure, but for a high shear rate ($\dot{\gamma} = 1000 \text{ s}^{-1}$).
 c) Strong attractive forces in state C ($I = 25 \text{ mmol/l}$): For low shear rates ($\dot{\gamma} = 50 \text{ s}^{-1}$) only one central cluster is formed, which is deformed slowly.

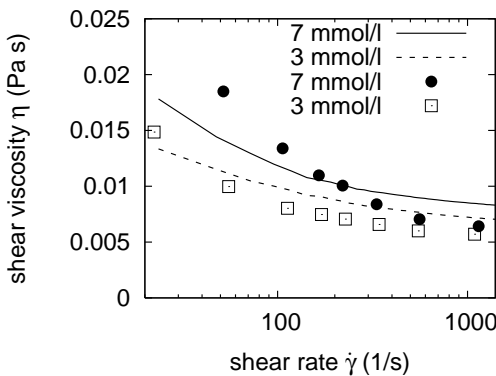


FIG. 6: Comparison between simulation and experiment: viscosity in dependence of the shear rate, for the states A ($I = 3 \text{ mmol/l}$) and B ($I = 7 \text{ mmol/l}$) of Fig. 1. Note: shear thinning is more pronounced for the slightly attractive interactions in state B than for the suspended state A. Lines denote experimental data [17], points are results from our simulations.

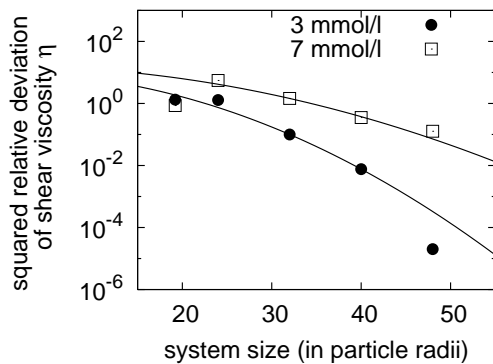


FIG. 7: Discrepancy between simulated viscosity and measurement for states A and B of Fig. 1 for different system sizes at low shear rates. The plot shows squared relative differences against z-extension of the simulation volume. The lines are a guide to the eye.

single point of Fig. 6 would need approximately 3000 CPU hours. For smaller shear rates or even deeper in the clustered regime of the phase diagram, e.g., in state C ($I = 25 \text{ mmol/l}$), the finite size effects become more pronounced, ending up in the extreme case of existing only one big cluster in the system. For simulations with good accuracy the effort again increases at least by the same factor.

Another argument are the limitations of the DLVO theory. DLVO potentials are derived for dilute suspensions and hence large particle distances. This is not fulfilled in our case (and even less inside the clusters). We are not aware of any theoretical attempt that overcomes this limitation. Nevertheless, the overall behavior can be reproduced by the simulation on a semi-quantitative level. In the simulations shear rates up to 2000 s^{-1} can be realized before limitations of the simulation method influence the results.

We have carried out simulations in the repulsive region of the phase diagram as well. We find layers parallel to the shear plane in analogy to Fig. 5b). In contrast to the suspended phase, in the repulsive regime the layer structure is present, at least locally, even if no shear is applied. If shear flow is present, the shear plane marks one orientation which the layer structure adopts. In some cases for very low ionic strengths one can observe shear bands so that the velocity gradient and thus the viscosity as well vary strongly in the system. Again, in the experiment, physical dimensions are much larger and on that length scale the velocity profile might be assumed to be linear when enough shear bands are in the system. The shear force and hence the viscosity rise with respect to the suspended phase, due to electrostatic repulsion. One can consider the particles together with the interaction range as soft spheres with an effective radius of the interaction range of the electrostatic repulsion. This

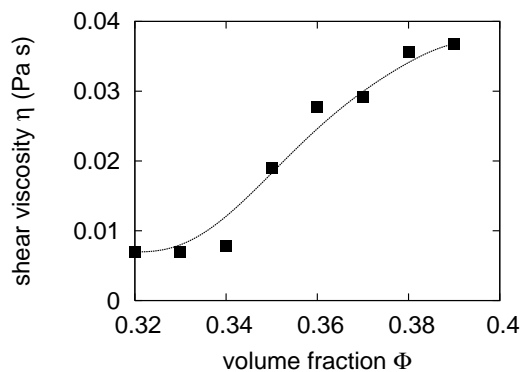


FIG. 8: Viscosity versus volume fraction for the repulsive region ($\text{pH} = 6$ and $I = 0.3 \text{ mMol/l}$). The shear rate was $\gamma = 100 \text{ s}^{-1}$. The points are simulation results, the line is a guide to the eye.

effective radius can be in our case about 25% larger than the particle radius. Therefore, a phase transition to a repulsive structure occurs in our system already between 35% and 40% volume fraction. Because of the smooth shape of the exponentially screened Coulomb potential it is not a sharp glass transition as for hard spheres, but smooth and shear rate dependent as well. In Fig. 8 we have shown the dependence of the viscosity on the volume fraction for $\text{pH} = 6$ and $I = 0.3 \text{ mMol/l}$. Starting at $\Phi = 0.34$ the shear viscosity starts to increase and reaches a value one decade larger beyond $\Phi = 0.4$.

V III. SUMMARY

We have shown how to relate DLVO poten-

tials to the conditions in a real aqueous suspension of Al_2O_3 particles. The behavior of shear viscosity has been studied in experiments and in simulations. We have found shear thinning due to a layer formation on the microscopic scale in the case of a suspension. If a clustered system is sheared, clusters are broken up into pieces by the imposed shear, which leads to a stronger shear thinning than in the suspended case. Close to the phase border we are able to reproduce the measured shear viscosity in the simulation.

Acknowledgments

This work has been funded by the German Research Foundation (DFG) within the project DFG-FOR 371 "Pelbide". We thank G. Gudelius, G. Huber, M. Kulzer, L. Hamau, and S. Richter for valuable collaboration.

Parts of this work are resulting from the collaboration with the group of A. Coniglio, Naples, Italy. M. Hecht thanks him and his group for his hospitality and for the valuable support during his stay there. M. Hecht thanks the DAAD for the scholarship (Doktorandenstipendium) which enabled him the stay.

M. Bier is deeply indebted to Dr. M. Biesheuvel and Dr. S.-H. Behrens for helpful discussions on charge regulation models.

[1] M. Hecht, J. Harting, T. Ihle, and H. J. Herrmann, *Physical Review E* 72, 011408 (2005).
 [2] M. Hutter, *Journal of Colloid and Interface Science* 231, 337 (2000).
 [3] W. B. Russel, D. A. Saville, and W. Schowalter, *Colloidal Dispersions* (Cambridge Univ. Press, Cambridge, 1995).
 [4] J. A. Lewis, *J. Am. Ceram. Soc.* 83, 2341 (2000).
 [5] L. Bocquet, E. Trizac, and M. Aubouy, *J. Chem. Phys.* 117, 8138 (2002).
 [6] M. Hutter, Ph.D. thesis, Swiss Federal Institute of Technology Zurich (1999).
 [7] A. M. Alevanets and R. Kapral, *J. Chem. Phys.* 110, 8605 (1999).
 [8] A. M. Alevanets and R. Kapral, *J. Chem. Phys.* 112, 7260 (2000).
 [9] Y. Inoue, Y. Chen, and H. Ohashi, *J. Stat. Phys.* 107, 85 (2002).
 [10] M. Ripoll, K. M. Ussawi, R. G. Winkler, and G. Gompper, *Europhys. Lett.* 68, 106 (2004).
 [11] M. Ripoll, K. M. Ussawi, R. G. Winkler, and G. Gompper, *Physical Review E* 72, 016701 (2005).
 [12] E. Falk, J. M. Lahtinen, I. Vattulainen, and T. Ala-Nissila, *Eur. Phys. J. E* 13, 267 (2004).
 [13] R. G. Winkler, K. M. Ussawi, M. Ripoll, and G. Gompper, *J. of Physics-Condensed Matter* 16, S3941 (2004).
 [14] P. Debye and E. Huckel, *Phys. Z.* 24, 185 (1923).
 [15] D. M. Quinn, *Statistical mechanics* (Univ. Science Books, Sausalito, 2000).
 [16] D. Chan, J. Perram, L. White, and T. Healy, *J. Chem. Soc. Faraday Trans. I* 78, 1046 (1975).

- [17] J. Reinshagen, R. C. D. Cruz, R. Oberacker, and J. Homann, submitted (2005).
- [18] J. Vermant and M. J. Solomon, *J. Phys.: Condens. Matter* 17, R187 (2005).
- [19] Thus, to calculate the local temperature in the cell under consideration one has to sum over the squares of the expression enclosed in square brackets.
- [20] in our case here it is 250 times smaller
- [21] e.g. we have not implemented other modes of lubrication than the "squeezing mode" (Eq.3)
- [22] clustering is already too strong in state B at $\tau = 20$ s to reasonably determine a viscosity and the system size dependence becomes too small for $\tau = 50$ s in state A.